SMA TECHNICAL MEMO 127

Date: 16 October 1998

Lunar and Planetary Fluxes at 230 GHz: Models for the Haystack 15-m Baseline

Mark A. Gurwell

ABSTRACT

We model the whole-disk and resolved fluxes for the limb of the moon, Mars, Jupiter, Saturn, Uranus, and Neptune for the 15-meter E-W baseline at the Submillimeter Array Haystack site. The period covered is for 1 October 1998 through 1 April 1999, the best months for observing in the 1mm band from that location. The moon and planets are strong continuum sources that have well-defined visibility functions under reasonable assumptions regarding their brightness distributions. While the modeling is approximate, particularly for the most resolved bodies, these results are useful for planning test observations and calibrating the SMA in both single-dish and interferometer modes.

1. Introduction

Initial testing and calibration of the SMA system, from antenna through correlator output, is best done using strong astronomical signals where the theoretical result is known *a priori*. Differences between the expected and measured visibility data sets can be used to pinpoint many errors and inaccuracies in the full system. With the SMA test system at Haystack Observatory, "strong" refers to very strong sources which can be observed through the local atmosphere, which usually has a high opacity and may have a short coherence timescale from turbulence. While point sources (e.g. quasars) provide excellent test signals in terms of their well-defined visibility functions, no quasar has an adequately large flux at 230 GHz. 3C273, usually the strongest quasar in the 1mm band, has a measured continuum flux of 15–20 Jy over the last year (as determined from the OVRO flux history database). While observable, stronger continuum sources would be more useful for testing purposes.

The brightest continuum sources in the 1mm band are the sun, moon, and planets (in that order), primarily due to their large sizes. In this work we examine the expected unresolved and resolved fluxes of these bodies and their suitability as calibration sources for testing the SMA system.

2. Parameters that Affect the Modeling of Thermal Emission

In order to accurately model lunar and planetary fluxes and visibility functions, it is necessary to know three important sets of information: observing parameters (such as baseline and field of view), planetary orbital (ephemeris) data, and planetary brightness temperatures and limb darkening functions.

2.1. The SMA Two-Element Interferometer at Haystack

The SMA assembly building and test pads are located in the general region of the Haystack Observatory 37-meter radio antenna, at +71.488 west longitude, +42.623 latitude. For local testing of the two-element interferometer, two of the four pads will be utilized, forming a 15-meter, east-west oriented baseline. The SMA antennas are 6 meters in diameter; therefore the usable range of projected baseline length (for no shadowing) is 6-m to 15-m, with the shortest spacings occurring at the lowest source elevations, and the maximum 15-m spacing occurring at source transit.

For operation at 230 GHz ($\lambda = 1.3$ mm), these baseline limits correspond to fringe spacings (λ/B) of $17.8''$ at 15 meters and $44.7''$ at 6 meters. The measured primary beam size of SMA antenna 2 is $52''$ FWHM at 230 GHz (Patel, private communication). This is larger than the beam size for a uniformly illuminated circular aperture ($1.02\lambda/D = 45.5''$) due to tapering of the illumination pattern.

As detailed in SMA Memo 123, typical conditions during the late fall and winter at the Haystack site indicate that the mean atmospheric zenith opacity will be approximately 0.5, and will be significantly smaller on many occasions. However, this opacity is very large relative to average conditions at the permanent Mauna Kea site where the system is designed to operate.

2.2. Lunar and Planetary Ephemeris Data

Detailed observations and predictions of the motions of the sun, moon, and planets are some of the oldest forms of astronomy. For purposes of modeling of visibility functions, the important parameters are source distance and declination at the time specified: distance provides the apparent size of the source, and declination (along with the observatory latitude) determine the time-variation of the instantaneous baseline projected on the source (the instantaneous $u - v$ location of the baseline). Extremely

accurate prediction ephemerides for the planets can be obtained via telnet or an Internet web browser from the JPL Solar System Dynamics Group HORIZONS System (see http://ssd.jpl.nasa.gov/horizons.html).

Figure 1 presents the motions of the sun, Mars, Jupiter, Saturn, Uranus, and Neptune in geocentric RA-DEC coordinates for the period 25 September 1998 through 02 April 1999. The position of the moon is not shown since it makes approximately 7.5 orbits during this period and would confuse the graph. For nearly the entire period of interest, Venus is within 30° of the Sun, and therefore has not been included in our list of possible targets.

2.3. Planetary Parameters

Table 1 presents useful statistics for the planets of interest, including equatorial, polar, and geometric mean diameters, and whole disk brightness temperatures at 230 GHz. These parameters are used in modeling the expected flux and visibility functions.

TABLE 1. Planetary Parameters

Planet	Equatorial Radius (km)[1]	Polar Radius (km)[1]	Geo. Mean Radius (km)	T_B(K) at 230 GHz[2]	T_B Reference
Mars	3393	3373	3383	200 (var)	Rudy et al. 1987
Jupiter	71492	66854	69134	165±7	Ulich et al. 1984
Saturn	60278	54364	57245	143±17	Courtin et al. 1977
Uranus	25559	24973	25264	101±4	Ulich et al. 1984
Neptune	24766	24342	24543	75±4	Ulich et al. 1984, Gurwell (unpub.)

[1] Beatty and Chaikin 1990

[2] Brightness temperatures are whole-disk averages

Figure 2 presents the variation of the apparent geometric mean diameter (in arcseconds) as a function of time throughout the period 25 September 1998 to 02 April 1999. Note the use of the logarithmic scale for diameter in the figure. As expected, the apparent size of Uranus and Neptune do not vary much, while Jupiter and Saturn exhibit moderate decreases in size through the period. Mars rapidly increases in size as it approaches opposition (24.67 April 1999).

2.3.1. Special Cases

Mars: The whole-disk brightness temperature of Mars is a function of its orbital season (L_S) and the geometry of the Earth–Mars–Sun system at the time of the observation. Since Mars has a very thin atmosphere, the diurnal variation of surface temperature (and subsequently of emitted brightness) is very significant. Radiative balance thermal modeling coupled with radiative transfer modeling at millimeter wavelengths has been presented in depth by Rudy et al. 1987; the model described in that work is available on the SMA workstation yoda.harvard.edu (contact M. Gurwell for access). For the work presented in the following sections we have assumed a mean brightness temperature of 200 K for Mars. The actually whole-disk temperature could vary by as much as 25% from this value.

Neptune: Uranus and Neptune have very similar continuum temperatures as a function of frequency throughout the millimeter and submillimeter, with one important exception: strong, extremely wide absorption lines due to CO rotational transitions have been measured (Gurwell, in preparation). The (2–1) line is roughly Lorentzian in shape, with an approximate 5 GHz FWHM, and a maximum absorption of ∼25% of the continuum, leading to a 230 GHz temperature of ∼75 K. Temperatures roughly 15 GHz to either side of the rest frequency are on the order of 100 K.

Jupiter and Saturn: Of the planets listed in Table 1, only these two objects have large oblateness ($\varepsilon = 1 - R_P/R_E$). For an interferometer, the visibility function will change depending on the orientation of the projected baseline relative to the polar axis of the planet (described by the north pole position angle), since the planet is larger in one dimension than the other. However, because the Haystack baseline is oriented E-W and all the planets are within 25° of the celestial equator (traveling along the ecliptic), there is only minor change in baseline orientation relative to the pole angle during a track, particularly when the source is within a few hours of transit. Therefore, for this work we have modeled each planet as a circularly symmetric disk using the apparent geometric mean radius.

2.3.2. Limb Darkening

Limb darkening (e.g. a decrease in observed intensity as a function of apparent radius from disk center) is a small but important feature of planetary brightness distributions. A planet with limb darkening will appear "smaller" than a uniformly bright disk of equal size, in terms of the location of the nulls ("zero-crossings") of the visibility function. In addition, the total flux from a limb darkened planet will be less than for a uniformly bright disk with equal disk-center intensity.

The variation of brightness from disk center to limb varies for each planet and often with frequency. In most cases, however, the amount of limb darkening is not a major influence except near the limb of the planet. For planets with small apparent size (Uranus and Neptune, and for part of the time Mars) the short baseline of the SMA Haystack site does not provide enough resolution to easily discern the limb darkening function. For Jupiter, which nearly fills the primary beam, the down-weighting of the planetary limb brightness by the primary beam pattern is a more important effect than limb darkening. Saturn and Mars are in the mid-range, and have sizes that approach the highest resolution on the 15-m baseline, and yet are only a small to moderate fraction of the beam size. As a result, modeling of the visibility functions for these two objects are most sensitive to the limb darkening function assumed. However, both Mars and Saturn are more complex than the other planets in terms of visibility functions: the surface temperature of Mars is highly non-uniform due to diurnal, latitudinal, and seasonal effects (e.g. day-night warming, presence of polar caps, etc.), and Saturn is very oblate and has a large ring system. Therefore, for all the planets we adopt the same limb darkening function which is approximately correct for the giant planets. The function itself has no direct theoretical basis, but is a simple and convenient formalism:

$$\frac{I(\rho)}{I(0)} \approx \cos^x \theta(\rho) = \left(1 - \rho^2\right)^{x/2} \tag{1}$$

where $\rho = r/R$ = fractional radius and θ = local emission angle relative to normal. As $x \to 0$ the limb darkened disk approaches a uniform disk; in this work we have taken $x = 0.05$. Integrating this function over a unit area disk gives the ratio of the disk-average intensity to the disk-center intensity, which can be shown to be $2/(2 + x)$, or roughly 0.976 for our choice of x.

3. Whole-Disk Flux Models for the Planets

Modeling of the whole-disk (or "zero-spacing") flux for all the planets follows the assumptions of circular symmetry, a common limb darkening function, and a Gaussian primary beam with FWHM $\theta = 52''$. The apparent planetary size varies with distance, and therefore time, as shown in Figure 2. Due to limb darkening, the disk center brightness temperature is greater than the whole-disk brightness temperature (Table 1) by 2.5%.

The whole disk flux is calculated by integrating the intensity, including limb darkening and primary beam weighting effects, over the disk of the planet (apparent radius R):

$$F = \int_0^{2\pi} \int_0^R I(r) r dr d\phi = 2\pi I(0) \int_0^R \left(1 - r^2/R^2\right)^{x/2} e^{-4 \ln 2 r^2/\theta^2} r dr \tag{2}$$

where I is intensity. This function is numerically integrated for each chosen time step, and results (both with and without primary beam weighting) are presented in Figure 3. As expected, on Jupiter exhibits a large difference in flux due to the primary beam pattern. Even so, the whole-disk flux of Jupiter is several thousand Janskys, and Saturn is more than 1000 Jy. Mars varies by an order of magnitude over the time-frame shown, from approximately 100 to 1000 Jy. Uranus and Neptune are much more modest, with average whole-disk fluxes of 36 and 10.7 Jy, respectively.

4. Visibility Models for the Planets

The visibility function model in all the cases we are considering in this work is the Fourier transform of a circularly symmetric disk with radius R (here variables have been transferred into polar coordinates):

$$\begin{aligned} V(u,v) &= \int_{\phi=0}^{2\pi}\int_{r=0}^{R} I(r)e^{-i2\pi r(u\cos\phi+v\sin\phi)}rdrd\phi \\ &= 2\pi\int_{r=0}^{R} I(r)J_0(2\pi\sqrt{u^2+v^2}r)rdr \qquad \text{[Hankel transform]} \end{aligned} \tag{3}$$

In the simple case of a uniformly bright disk

$$V(u,v) \;=\; I(\nu,T_B)\;\pi R^2\;\frac{J_1\left(2\pi\beta\right)}{\pi\beta} \tag{4}$$

where $\beta = \sqrt{u^2+v^2}\;R$, equivalent to the ratio of the apparent radius to the projected baseline fringe spacing. Note that as $\beta \to 0$, the visibility approaches the whole-disk flux (i.e. $\lim_{x\to 0} J_1(2x)/x = 1$). The location of nulls, or zero-crossings of the visibility function, are precisely known values of β, and therefore of the apparent size of the uniform disk; the first null occurs at $\beta = 0.6098$.

For our models, each source is circularly symmetric and located (presumably) at the phase center, and therefore the visibility function is a real function, with positive and negative amplitude (or alternatively, 0° and 180° phase), depending on the value of β and the amount of limb darkening.

Visibility function models were calculated for Mars, Jupiter, Saturn, Uranus, and Neptune for seven dates ($0^{\rm h}$ UT on the first day of each month, October 1998 through April 1999). For each date the declination and apparent geometric mean size were determined from ephemeris data, and $u-v$ points were calculated for the 15-m Haystack baseline for that declination as a function of time relative to source transit. Points when the source was

below 15°, or when the projected baseline was less than 6 meters (corresponding to partial antenna shadowing) were omitted. Results from these calculations are shown in Figures 4-8.

5. Visibility Model for the Lunar Limb

The moon presents a tremendous source of continuum flux on very short baselines. Taking a mean value of the lunar brightness temperature of $\sim$ 200 K, the zero-spacing flux in the SMA 52″ primary beam at 230 GHz is 23500 Jy. However, on the 15-m Haystack baseline this flux is almost entirely resolved out.

The moon can still be a strong source for testing at the Haystack site, by observing the lunar limb. As shown in Figure 9, the small size of the SMA primary beam relatively to the size of the moon allows us to approximate the lunar limb as an infinite half-plane, weighted by a Gaussian field of view (the primary beam), i.e. an infinite "half-Gaussian" with a peak equal to the moon's limb brightness temperature.

Consider the case when the primary beam is centered on the west limb of the moon. We use x to signify a position in RA and y for DEC:

$$I(x,y) = \begin{cases} I_0(\nu, T_M)\ exp\left[-4\ln 2\ (x^2+y^2)/\theta^2\right] & x \geq 0 \quad (5a) \\ 0 & x < 0 \quad (5b) \end{cases}$$

The visibility function is then:

$$V(u,v) = \iint_{-\infty}^{+\infty} I(x,y) e^{-i2\pi(ux+vy)} dx\ dy \quad (6a)$$

$$= I_0 \int_0^{+\infty} e^{-4\ln 2\ x^2/\theta^2} \left(\cos(2\pi ux) - i\sin(2\pi ux)\right)\ dx \times 2\int_0^{+\infty} e^{-4\ln 2\ y^2/\theta^2} \cos(2\pi vy)\ dy \quad (6b)$$

$$= I_0 \left[\sqrt{\frac{\pi}{\ln 2}}\ \frac{\theta}{4}\ e^{-\pi^2\theta^2u^2/4\ln 2} - i\int_0^{+\infty} e^{-4\ln 2\ x^2/\theta^2} \sin(2\pi ux)\ dx\right] \times \sqrt{\frac{\pi}{\ln 2}}\ \frac{\theta}{2}\ e^{-\pi^2\theta^2v^2/4\ln 2} \quad (6c)$$

$$= I_0\ \frac{\pi\theta^2}{8\ln 2}\ e^{-\pi^2\theta^2(u^2+v^2)/4\ln 2} \times \left[1 - i\sqrt{\frac{\pi}{\ln 2}}\ \theta u\ {}_1F_1\left(\frac{1}{2};\frac{3}{2};\frac{\pi^2\theta^2u^2}{4\ln 2}\right)\right] \quad (6d)$$

where ${}_1F_1(\alpha;\gamma;z)$ is a confluent hyper-geometric function (see Gradshteyn and Ryzhik 1994, Eq. 3.896.3, pp 515). Note that as $u, v \rightarrow 0$ the visibility amplitude goes to the total flux of the half-Gaussian, as expected. For a $52''$ beam at 230 GHz, and assuming a mean lunar temperature of 200 K, this is 11750 Jy.

For this work we have chosen to use Eq. 7c and numerically integrate the Gaussian-sine integral. Results obtained for a range of u when v is assumed zero, as is the case for an E-W baseline when the source is transiting, are presented in Figure 10. This gives a feel for the magnitude of the resolved flux we can expect for a given baseline when observing the limb of the moon. We note that for baselines greater than about six meters, the visibility function is essentially all imaginary. The amplitude is greater than 1000 Jy for baselines less than about 19 meters.

This analysis shows that the visibility amplitude is maximized when the projected baseline is perpendicular to the limb of the moon (and the interferometer fringes are parallel to the limb); this is when $v = 0$ in the above case. Therefore, the point on the limb which is perpendicular to the instantaneous baseline at any time should be tracked to observe the maximum visibility. With the 15-m east-west baseline, however, the v-component of the baseline is relatively small, particularly near source transit; we therefore feel that tracking of either the east or west limb will provide an adequate signal, eliminating the need to track the perpendicular limb point.

Since the moon varies in declination rapidly, and makes approximately 7.5 transits around the Earth over our timeframe of interest, we have modeled the expected visibility function of the west limb of the moon for nine declinations: -20° to +20°. Again, the mean brightness temperature of the moon was used: the true brightness temperature of the west limb of the moon is dependent upon the lunar phase, though it should not vary by more than a factor of two from 200 K. The full u, v coverage was included, as for the planets, and results as a function of time relative to source transit are presented in Figure 11. At transit, all the declinations produce the same visibility amplitude, since the baseline has only a u component at that time, with a length of 15 meters. The flux at transit is approximately 1300 Jy. Before and after transit each declination causes a significantly different measure of the visibility with time. When the declination is near 0°, the visibility generally increases with the decreasing projected baseline, but for higher declinations it tends to decrease. In any event, the change in the visibility amplitude is relatively slow, and the very large flux makes the limb of the moon an attractive source for initial testing of the SMA system.

6. Conclusions

We have estimated the unresolved fluxes and resolved visibility amplitudes expected from interferometric observations of Mars, Jupiter, Saturn, Uranus, Neptune, and the west limb of the moon at 230 GHz for the 15-m E-W baseline at the SMA Haystack site. In general, the planets and moon are the brightest continuum sources in the sky (with the exception of the sun), even though significant flux is resolved out in the interferometric mode for some objects. These sources will be easily detectable with the two-element interferometer at Haystack in a short integration time, and will therefore be very useful sources for initial testing and calibration of the SMA system.

REFERENCES

Beatty, J.K., & Chaikin, A. 1990 The New Solar System (3rd edition), Cambridge University Press/Sky Publishing Corp, Cambridge, England and New York/Cambridge, MA

Chamberlain, J.W., & Hunten, D.M. 1987, Theory of Planetary Atmospheres, Academic Press, San Diego

Courtin, R., Coron, N., Gispert, R., Bruston, P., LeBlanc, L., Dambier, G., Vidal-Madjar, A., & Encrenaz, Th. 1977, A&A 60, 115-123

Gradshteyn, I.S., & Ryzhik, I.M. 1994, Table of Integrals, Series, and Products (5th edition, ed. by A. Jeffrey), Academic Press, San Diego

Rudy, D.J, Muhleman, D.O., Berge, G.L., Jakosky, B.M., & Christensen, P.R. 1987, Icarus 71, 159-177

Thompson, A.R., Moran, J.M., & Swenson, G.W., Jr. 1986, Interferometry and Synthesis in Radio Astronomy, John Wiley & Sons, New York

Ulich, B.L., Dickel, J.R., & DePater, I. 1984, Icarus 60, 590-598

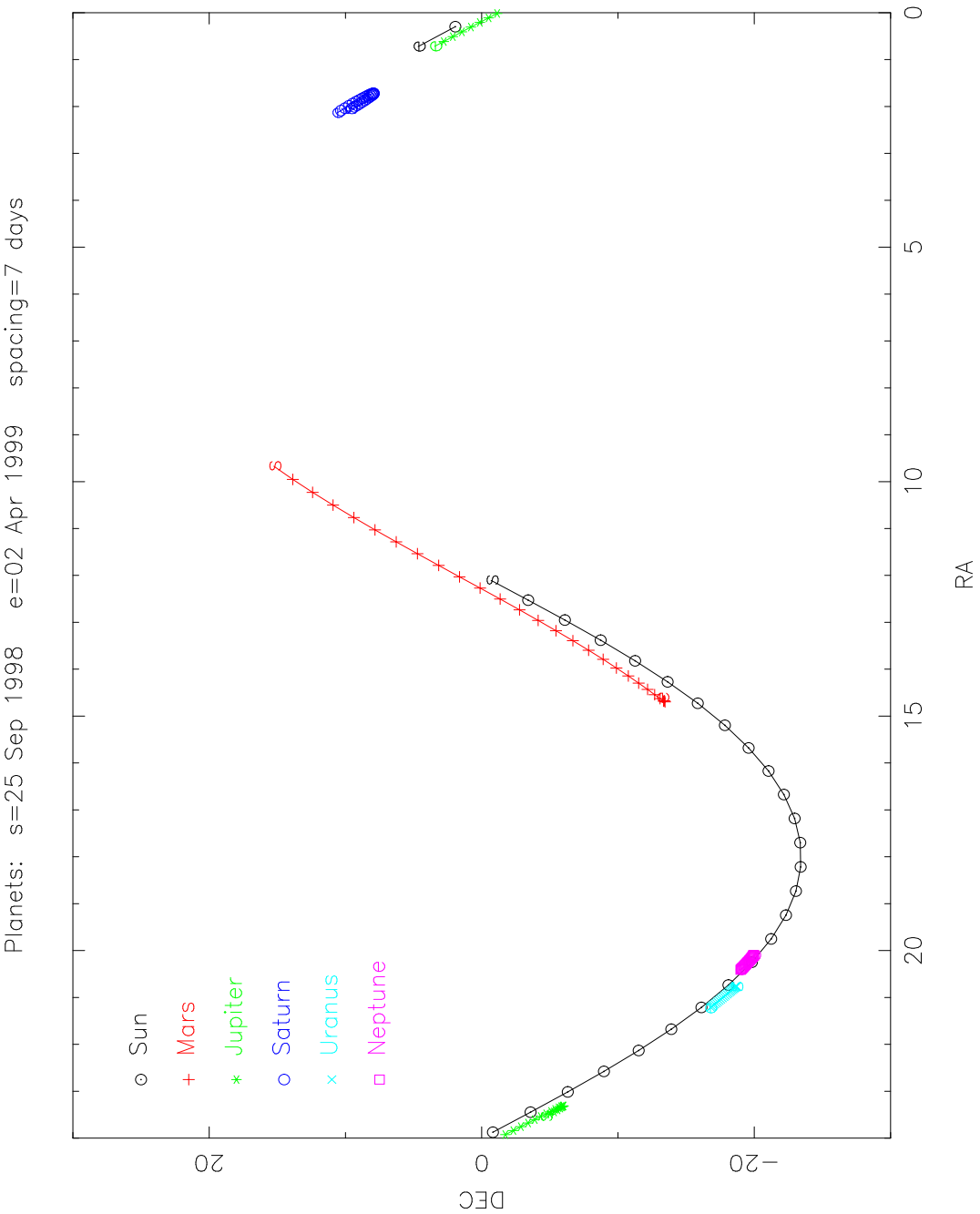

Figure 1. Geocentric RA-DEC motion of the Sun, Mars, Jupiter, Saturn, Uranus, and Neptune from 25 September 1998 through 02 April 1999.

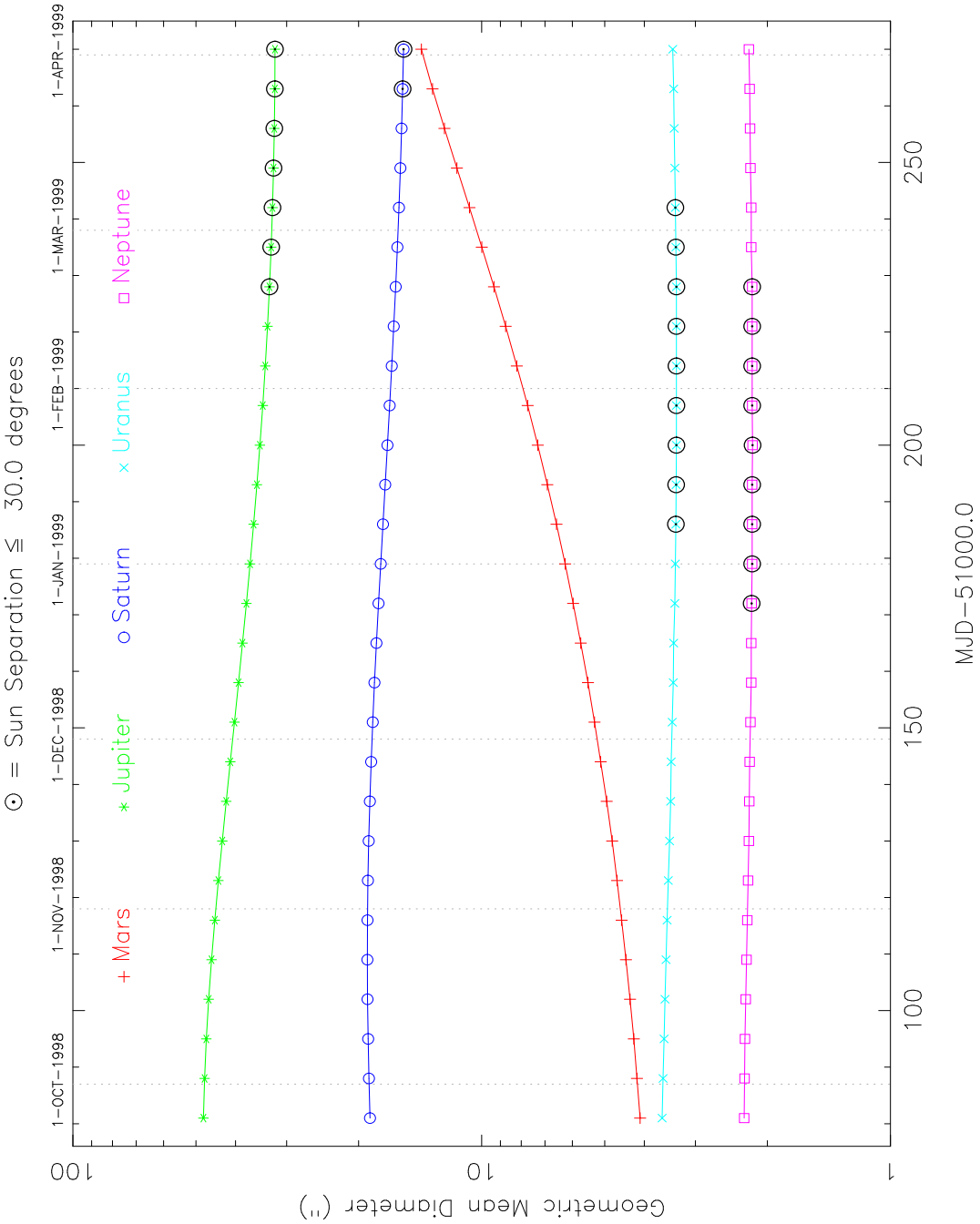

Figure 2. Apparent geometric mean diameters for Mars, Jupiter, Saturn, Uranus, and Neptune from 25 September 1998 through 02 April 1999.

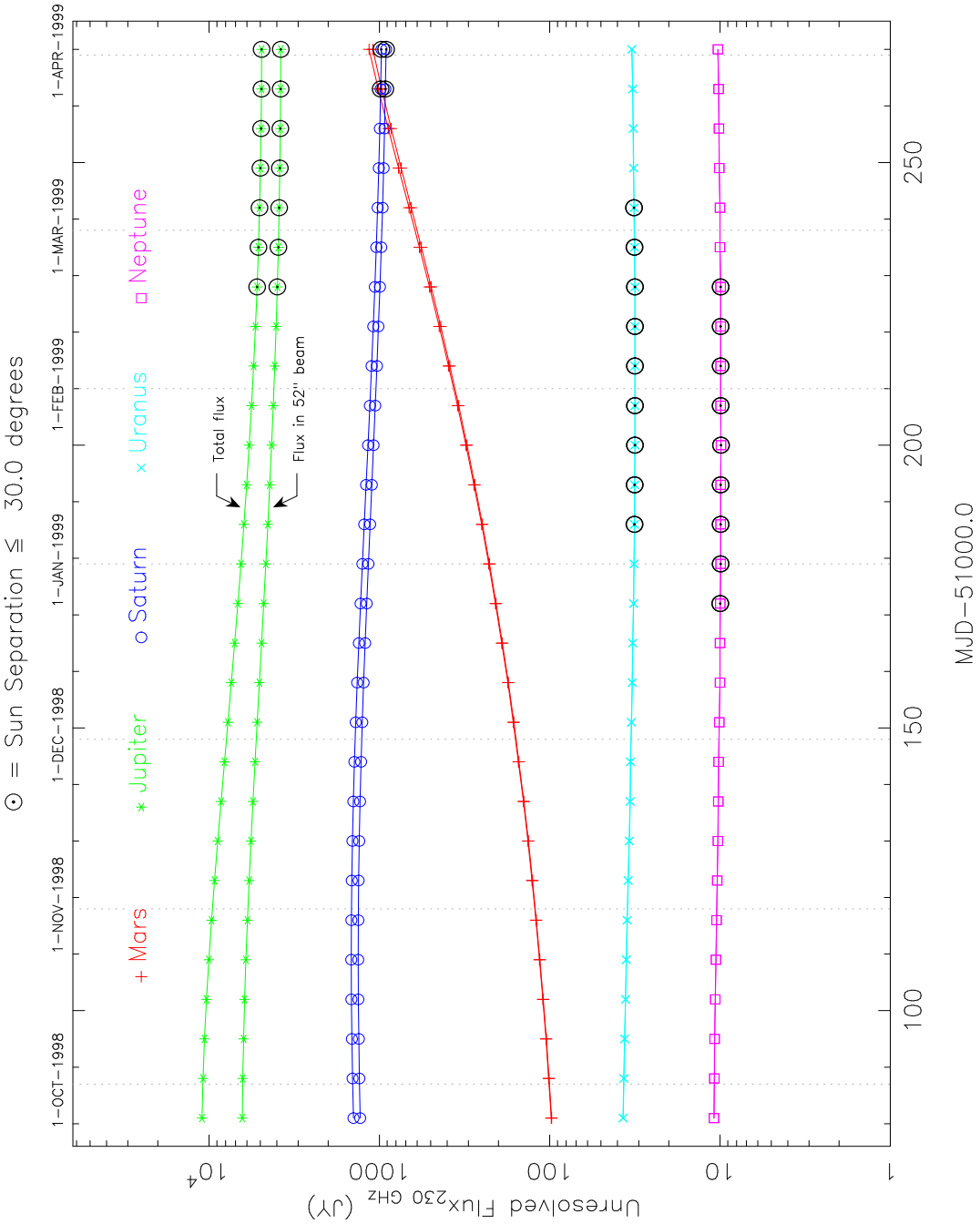

Figure 3. Model whole-disk fluxes at 230 GHz (with and without weighting by a 52″ FWHM primary beam) for Mars, Jupiter, Saturn, Uranus, and Neptune from 25 September 1998 through 02 April 1999.

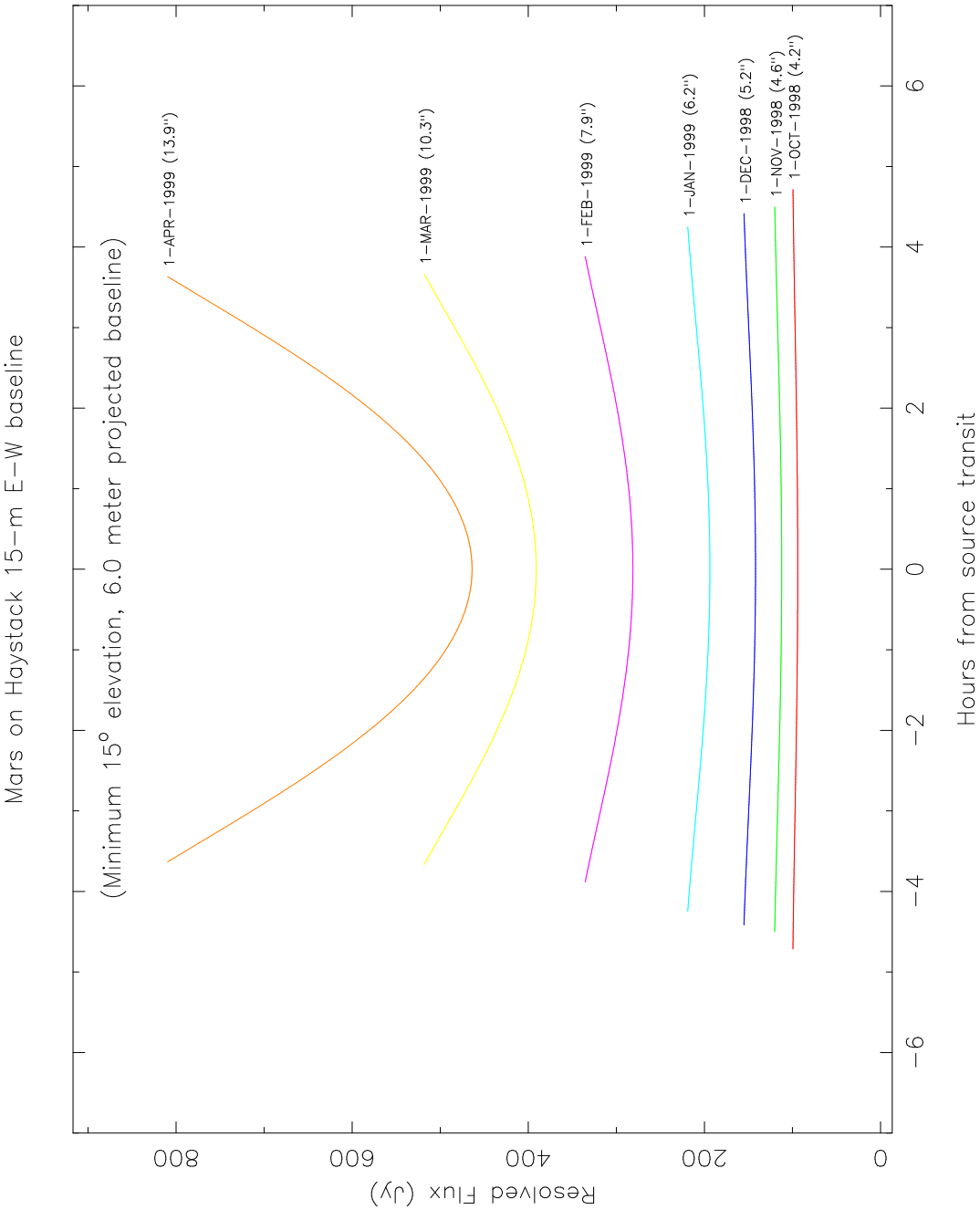

Figure 4. Model 230 GHz visibility amplitude for Mars as a function of time relative to source transit for the SMA Haystack 15-m baseline. Primary beam FWHM=52″.

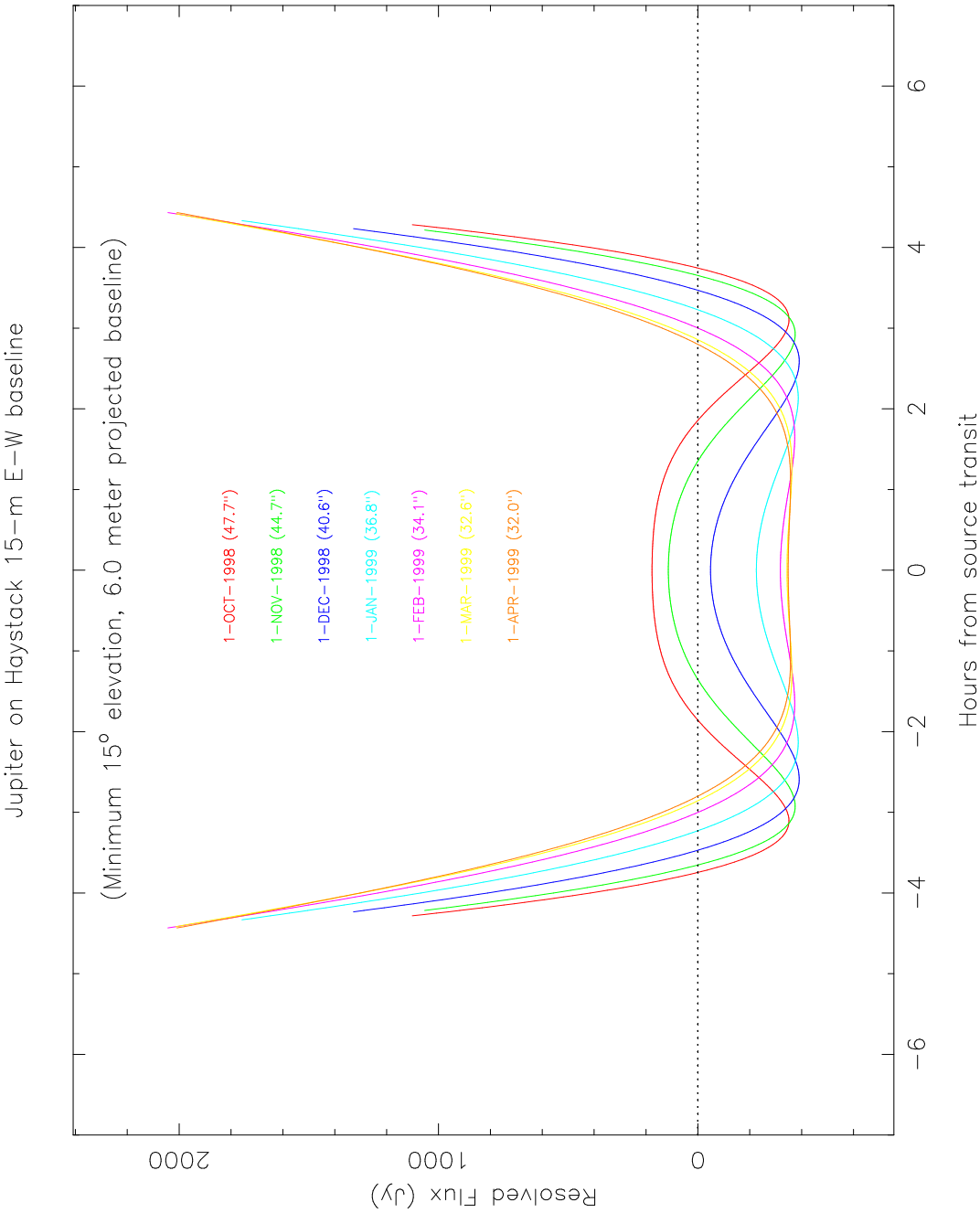

Figure 5. Model 230 GHz visibility amplitude for Jupiter as a function of time relative to source transit for the SMA Haystack 15-m baseline. Primary beam FWHM=52″. In this figure "negative" flux refers to visibility phase of 180°.

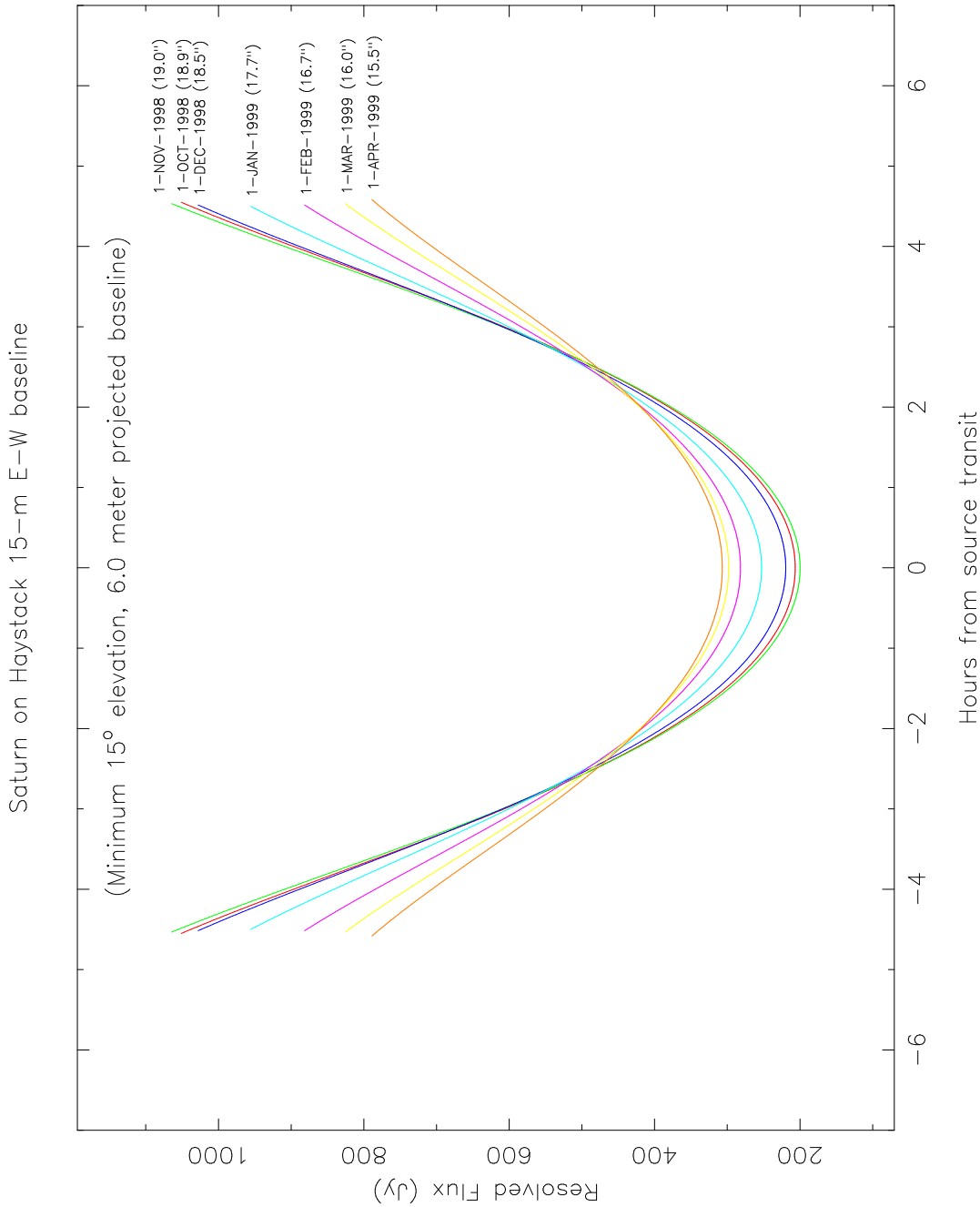

Figure 6. Model 230 GHz visibility amplitude for Saturn as a function of time relative to source transit for the SMA Haystack 15-m baseline. Primary beam FWHM=52″.

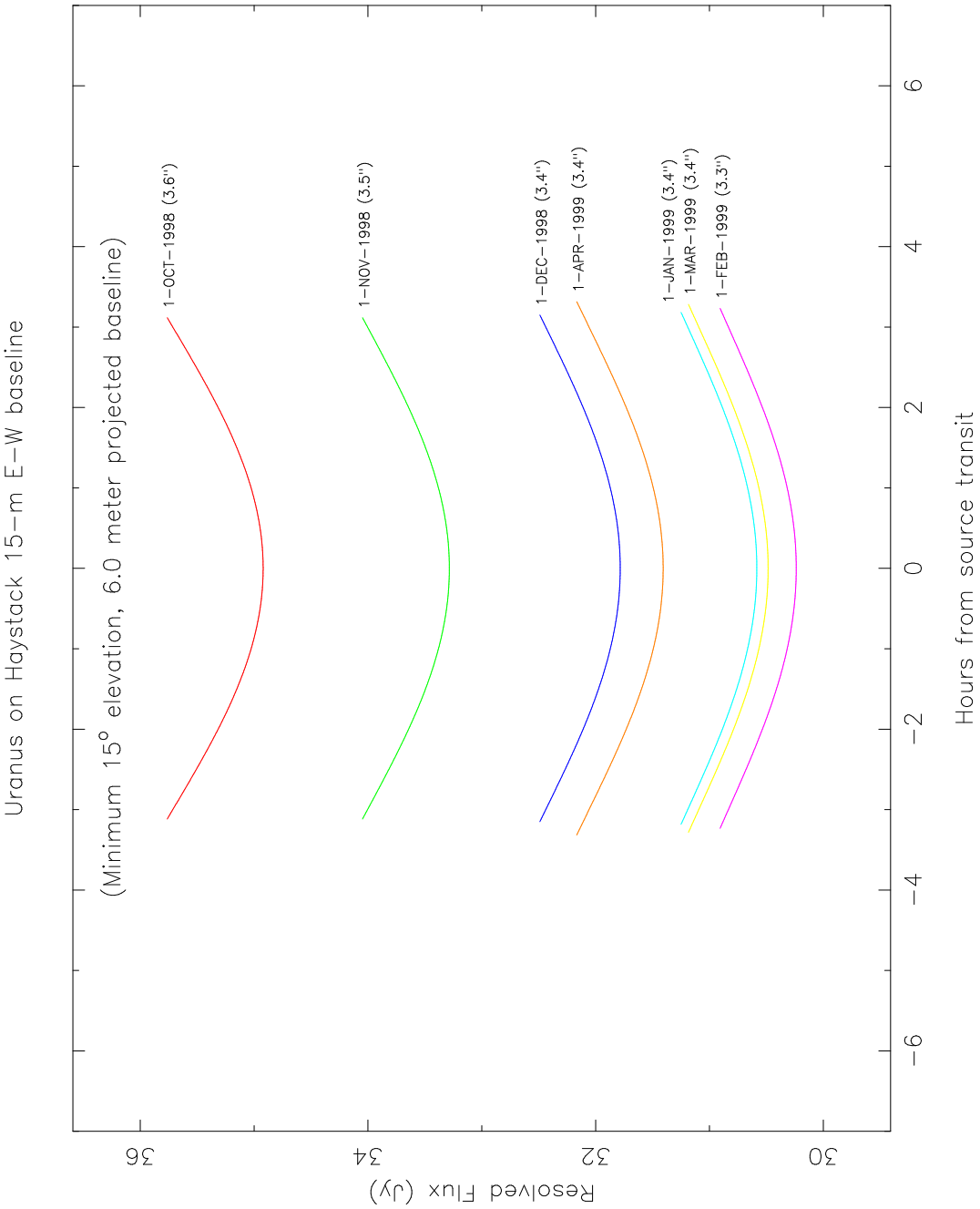

Figure 7. Model 230 GHz visibility amplitude for Uranus as a function of time relative to source transit for the SMA Haystack 15-m baseline. Primary beam FWHM=52″.

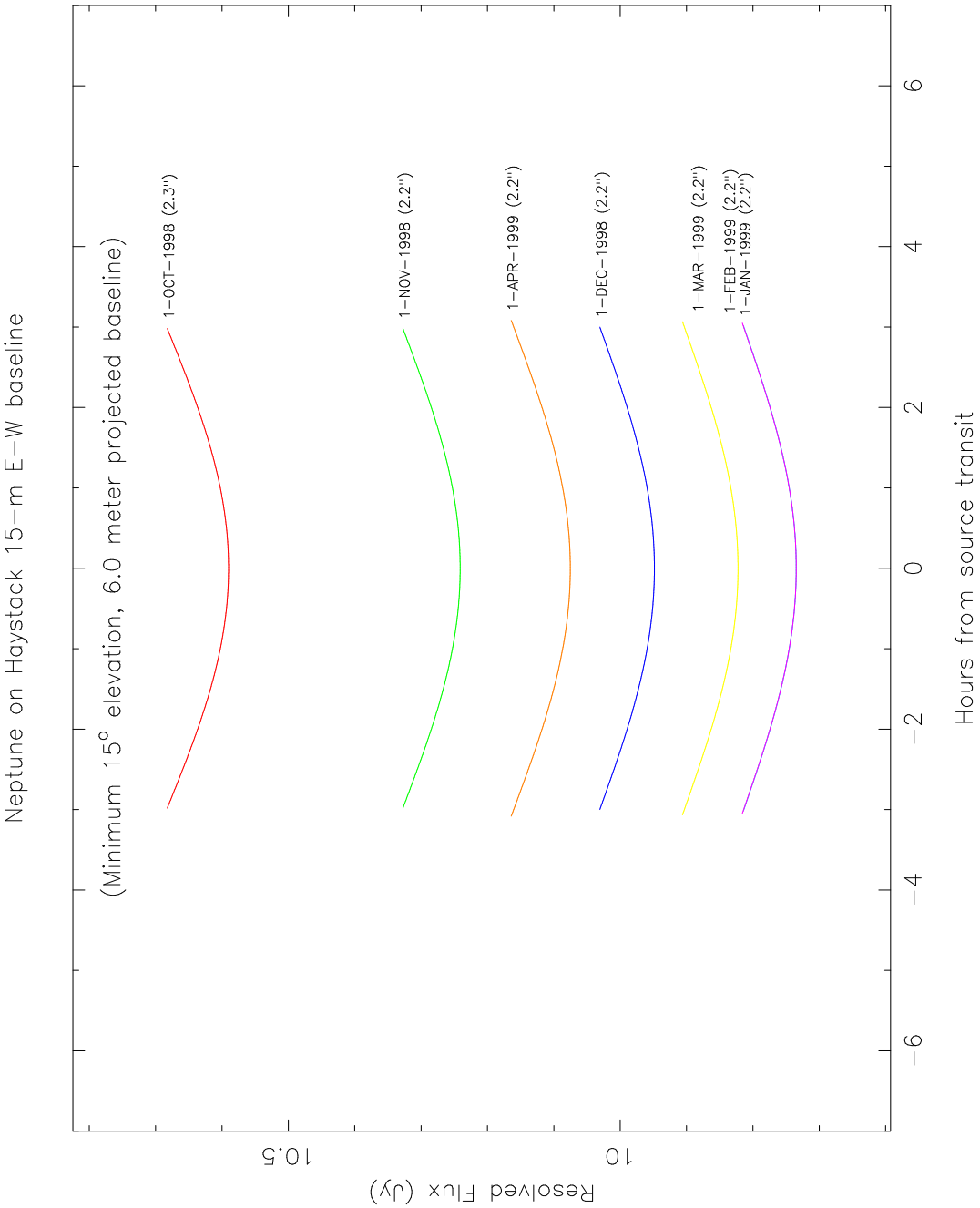

Figure 8. Model 230 GHz visibility amplitude for Neptune as a function of time relative to source transit for the SMA Haystack 15-m baseline. Primary beam FWHM=52″.

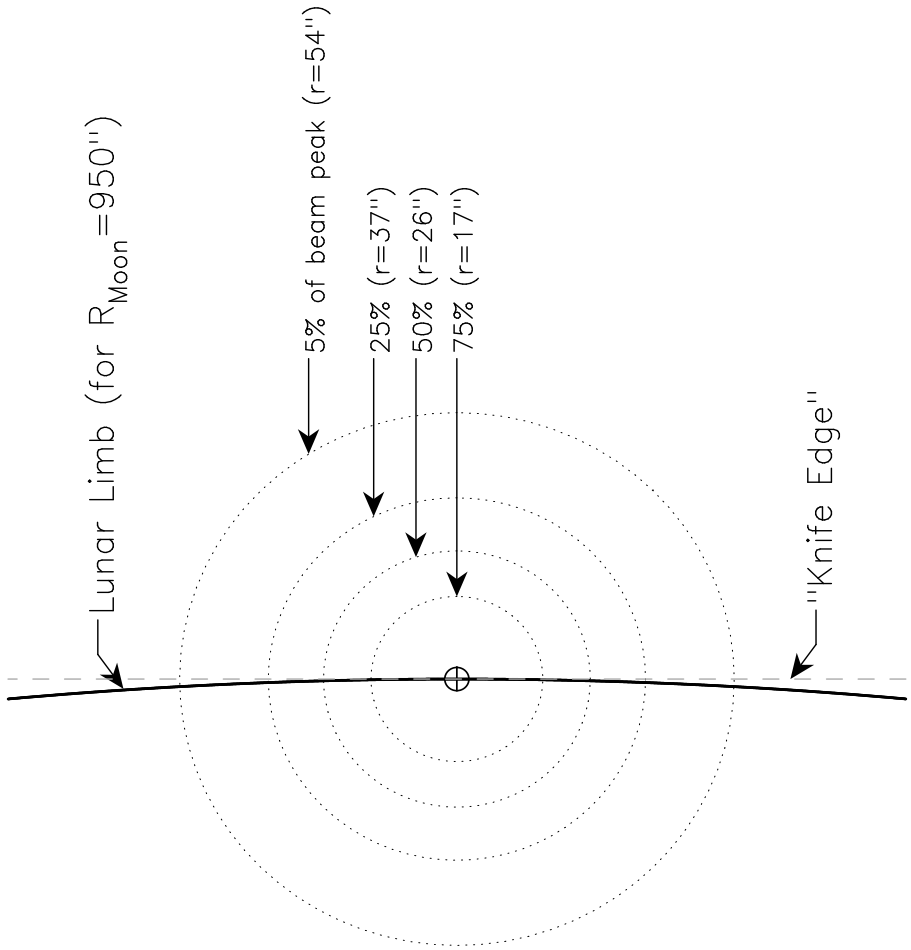

Figure 9. Relation of the SMA primary beam with the limb of the moon.

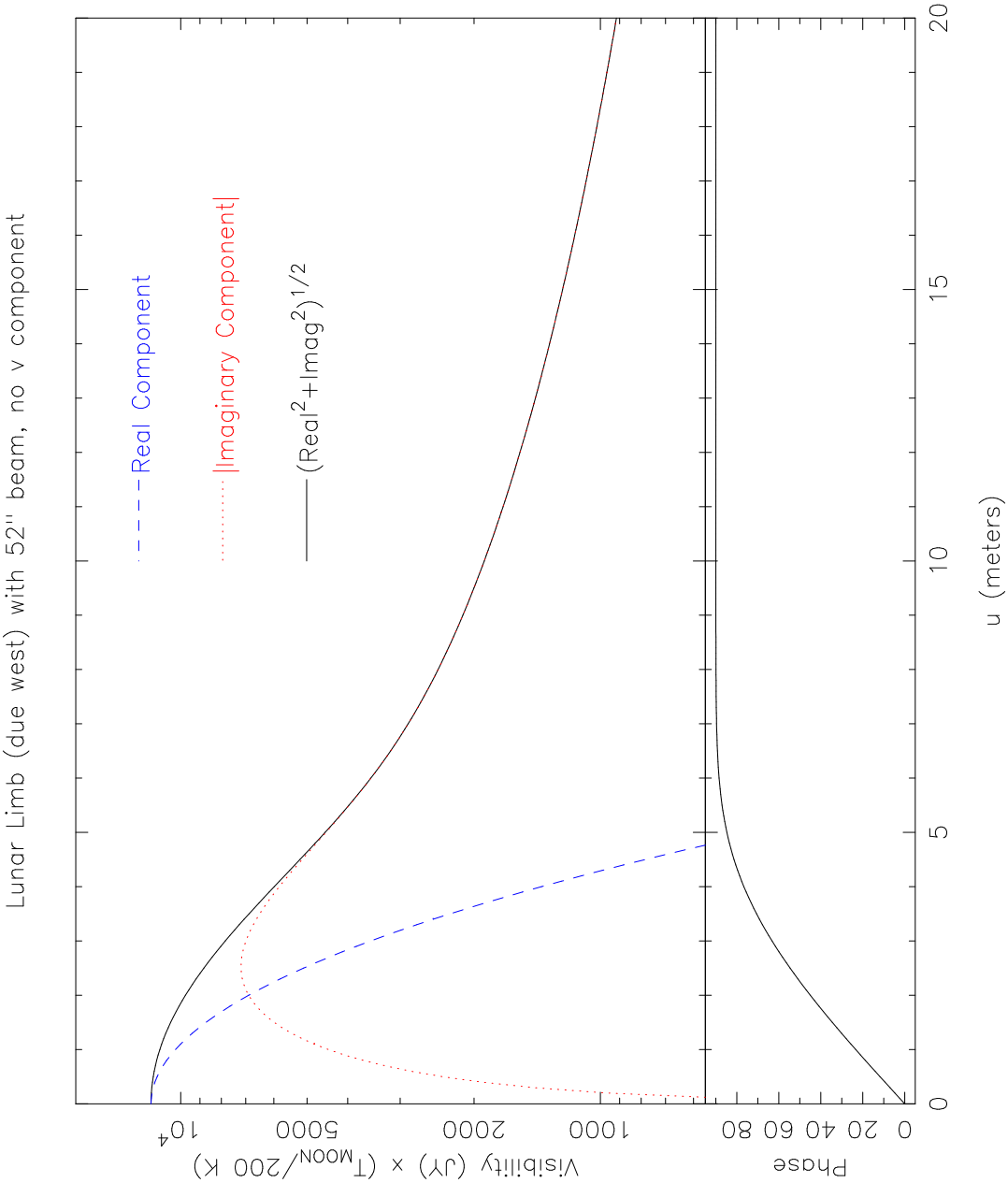

Figure 10. Model 230 GHz visibility amplitude for the west limb of the moon as a function of the baseline u-component, for $v = 0$. Primary beam FWHM=52″.

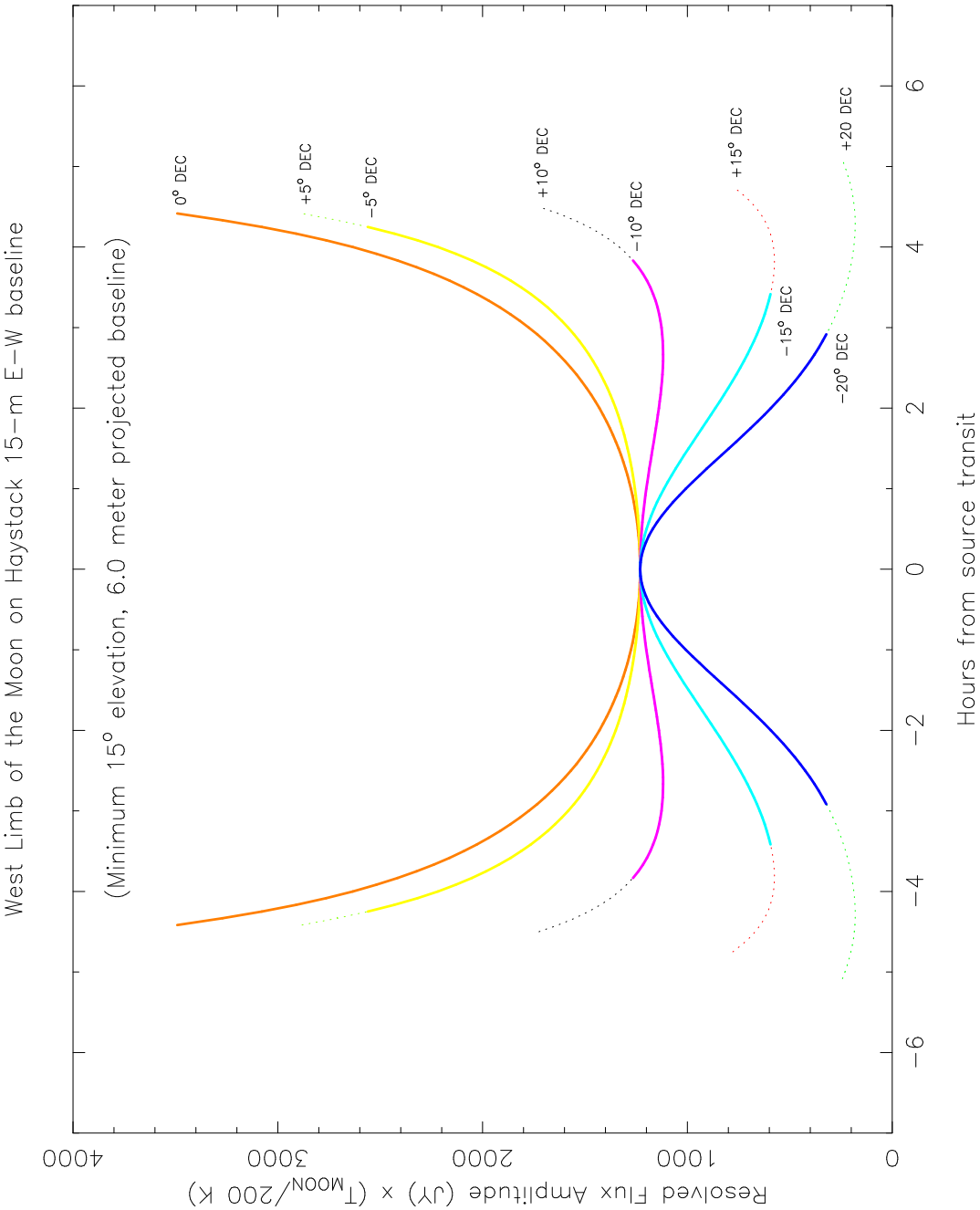

Figure 11. Model 230 GHz visibility amplitude for the west limb of the moon as a function of time relative to source transit for the SMA Haystack 15-m baseline, for 9 values of declination. Primary beam FWHM=52″.